DALHOUSIE UNIVERSITY

Version: Post-print

Influence of Geometry and Fiber Properties on Rupture Strain of Cylindrical FRP Jackets under Internal Ice Pressure

Pedram Sadeghian[1], Rudolf Seracino[2], Baishali Das[2], and Gregory Lucier[2]

[1] *Department of Civil and Resource Engineering, Dalhousie University, Halifax, NS, B3H 4R2, Canada.*

[2] *Department of Civil, Construction, and Environmental Engineering, North Carolina State University, Raleigh, NC 27695, USA.*

ABSTRACT

This paper presents an study on the rupture strain of cylindrical fiber-reinforced polymer (FRP) jackets under internal ice pressure. A total of 45 cylindrical FRP jackets were prepared using three unidirectional carbon, glass, and basalt fabrics in three different internal diameters, namely 60, 114, and 216 mm, and one-, two-, and three-plies. Three jackets for each combination were typically tested and the average hoop rupture strains were obtained and compared to the rupture strain of flat coupons in the form of a strain efficiency factor. It was found that the strain efficiency factor ranged from 0.53 to 1.05 with an average of 0.77. A new analytical model was also developed based on the bi-axial state of stress in a cylindrical FRP jacket to obtain the rupture strain and strain efficiency factor of the FRP jacket using a closed-form solution. The model engaged four major parameters, namely: diameter, thickness, axial/transverse strength ratio, and Poisson's ratio of the FRP jacket. The two latter parameters were eliminated after a parametric study to propose a simplified formula. The analytical and simplified models predicted the experimental strain efficiency factors with an average error of -3.4% and -4.6%, respectively.

1. INTRODUCTION

Fiber-reinforced polymer (FRP) composites have been extensively applied for the strengthening of existing reinforced concrete (RC) columns [1][2][3][4][5][6]. It is well-known that wrapping circular cross-sectional concrete columns with unidirectional FRPs in the circumferential (i.e. hoop) direction of the column is an effective method of strengthening. In this method, as the concrete core dilates under axial compressive loading, the FRP jacket confines the concrete core by inducing a uniform radial confining pressure [3][8][9][10][11][12][13]. It is also well-established that the tensile rupture of the FRP jacket in the hoop direction controls the behavior of the column [14][15][16][17][18]. Typically, the rupture of FRP in the hoop direction occurs at a strain level less than the rupture strain obtained from corresponding flat coupon tests [19][20][21][23][24]. The reduced rupture strain is factored into most existing confinement models, usually in the form of a strain efficiency factor, as proposed by Pessiki et al. [14], which is the ratio of the reduced rupture strain of the FRP jacket to the rupture strain from flat coupon tests. There are numerus studies trying to calibrate the strain efficiency factor based on concrete cylinders wrapped with FRPs. Table 1 summarizes some of the studies indicating that the strain efficiency factor varies significantly. The concept of the strain efficiency factor was implemented by the ACI 440.2R-17 [27] design guide as follows:

$$\kappa_\varepsilon = \frac{\varepsilon_{fe}}{\varepsilon_{fu}} \tag{1}$$

where ε_{fe} is the effective strain in the FRP jacket at failure, ε_{fu} is the design rupture strain of the FRP, and κ_ε is the strain efficiency factor. It should be noted that there are multiple studies indicating that the hoop strain varies over the surface of the FRP jacket. Bisby and Take [28] implemented an optical strain measurement technique to quantify the strain efficiency factor by measuring the variation in hoop strains over the surface of FRP jackets. It was found the hoop

strain is highly variable over the surface of an FRP-wrapped concrete cylinder, and that the coupon failure strain can be achieved only locally. It was shown that hoop strains over the surface of the FRP-wrapped cylinders at failure varied significantly. The highly-variable nature of the hoop strain was also reported by Smith et al. [21], Wu and Jiang [29], and El-Hacha and Abdelrahman [30].

Currently, ACI 440.2R-17 [27] uses a constant strain efficiency factor of 0.55 without providing any rational approach to quantify the strain efficiency factor. It provides two possible reasons for the strain efficiency and premature failure of FRP jackets in a FRP-wrapped concrete column, namely: the multi-axial state of stresses in the FRP jacket; and stress concentration regions caused by cracking of the concrete as it dilates. Lam and Teng [32] identified at least three factors affecting the premature FRP rupture, namely: the curvature of the FRP jacket; the deformation localization of the cracked concrete; and the existence of an overlapping zone.

Chen et al. [19] proposed additional contributing factors, namely: geometric imperfections of the concrete cylinder; non-uniform bonding of the FRP to the concrete cylinder; and geometric discontinuities at the ends of the FRP jacket. They concentrated on the third contributing factor using an elastic finite element analysis and identified the curvature of the FRP jacket as a significant factor. Later, Chen et al. [33] identified seventeen contributory factors possibly affecting the FRP rupture strain, ranging from geometrical discontinuity, triaxial stress states, geometrical imperfections, and non-uniform supports in test setup. Smith et al. [21] studied the effect of the number of FRP layers and different overlap locations. The effects of FRP wrapping scheme and overlap configuration were also studied by Vincent and Ozbakkaloglu [34] and Pham et al. [35]. Fraldi et al. [36] and Lignola et al. [37] considered the multi-axial state of stresses in FRP jackets due to the transfer of longitudinal load through the bond with concrete. Sadeghian and Fam [31] considered the bi-axial state of longitudinal and hoop stresses, ignoring the radial stress.

In order to provide reliable experimental measurements of the strain efficiency, De Caso y Basalo et al. [38] proposed a method to investigate the circumferential strain of FRP jackets known as the investigation of circumferential-strain experimental method (here after referred to as the ICE test method). This method simulates the lateral expansion of concrete core by employing water, which expands when it changes from liquid to solid (ice), as a medium to apply an internal hydrostatic pressure on cylindrical FRP jacket specimens. The average ultimate hoop strain from 54 cylindrical glass FRP jackets with varying diameter and laminate thickness clearly indicated a lower level of strain than those found in similar flat coupon specimens with an average strain efficiency factor of 0.72. It shows that the ICE test method can characterize the premature failure of FRP jackets in a more representative fashion than flat coupon tests. However, there is a lack of test data using the ICE test method, as well as a lack of a rational approach explaining the premature failure of FRP jackets even without a concrete core. However, as noted previously, there are other factors (e.g. the longitudinal stress of the column and concrete cracking due to dilation) affecting the strain efficiency of FRP-wrapped concrete that are not modeled in the ICE test method.

This paper presents an experimental study on the rupture strain and strain efficiency factor of cylindrical FRP jackets tested using the ICE test method. A total of 45 cylindrical FRP jackets were prepared using three unidirectional carbon, glass, and basalt fabrics in three different internal diameters, namely 60, 114 and 216 mm, and one-, two-, and three-plies. Also, an analytical model is developed based on the bi-axial state of stress in the FRP jacket due to a tensile stress in the hoop direction and a compressive stress in the radial direction. For typical FRP materials, the analytical model is simplified to a more applicable form as a function of the diameter/thickness

ratio (i.e. curvature) of the FRP jacket only. The results are verified against the experimental results.

2. EXPERIMENTAL PROGRAM

A total of 45 cylindrical hollow FRP jackets were prepared and tested using the ICE test method to quantify the hoop rupture strain of circular FRP jackets. In the ICE test method, as proposed by De Caso y Basalo et al. [38], an internal hydrostatic pressure is applied to a cylindrical FRP jacket simulating the lateral dilation of an FRP-wrapped concrete core under uniaxial load. The pressure is achieved using water which expands when it freezes. The test method is a simple closed-loop technique with minimum boundary effects for investigating the behavior of FRP jackets under pure hoop tension. The parameters investigated in the experimental program include: fiber type (carbon, glass, and basalt); inner diameter of the FRP jacket (60, 114, and 216 mm); and number of FRP layers (1, 2, and 3 layers). Flat coupon tests were also performed to obtain the rupture strain under uniaxial tension. The objective of the experimental program was to study the effect of fiber properties and jacket diameter and thickness on rupture strain of the FRP jackets. Selected jacket specimens were tested with five strain gauges along the circumference to capture the distribution of hoop strain at various locations in overlapped and non-overlapped portions of the FRP jacket. The objective of the selected jacket specimens was to locate the zones of strain concentration on the FRP jacket where rupture initiates, leading to premature failure.

2.1. Material Properties

2.1.1. Fibers

Three types of fibers were used in the experimental program: carbon, glass, and basalt.

Carbon Fibers: A 644 g/m^2 unidirectional fabric made of carbon fibers (1.74 g/cm^3) with reported tensile strength, modulus, and maximum elongation of 4,000 MPa, 230 GPa, and 1.7%, respectively [39].

Glass Fibers: A 915 g/m^2 unidirectional fabric made of glass fibers (2.55 g/cm^3) was used with reported tensile strength, modulus, and maximum elongation of 3,240 MPa, 72 GPa, and 4.5%, respectively [40].

Basalt Fibers: A 300 g/m^2 unidirectional fabric made of basalt fibers (2.65 g/cm^3) was used with reported tensile strength, modulus, and maximum elongation of 2,100 MPa, 91 GPa, and 2.3%, respectively.

2.1.2. Epoxy

An epoxy resin was used with reported properties (post-cured at 60 °C for 72 h) of tensile strength, modulus, and maximum elongation of 72.4 MPa, 3.18 GPa, and 5.0%, respectively [40].

2.2. Flat Coupon Tests

FRP sheets (300×300 mm) were manufactured using one and two layers of each fabric on a polyurethane plastic sheet. After 7 days of curing at room temperature, the FRP sheets were cut to 25×300 mm strips using a band saw. Three flat coupons from each fabric were prepared and tested according to ASTM D3039 [41]. Aluminum tabs (6.35×25×75 mm) were attached to all coupons using the epoxy resin for appropriate gripping and load distribution. Tension tests were performed using a 90 kN capacity universal testing machine with a 50-mm extensometer to measure the strain of the FRP coupons during testing. It was observed that all three FRP materials had a linear behavior up to tensile rupture. A summary of test results is presented in Table 2. It shows that the average rupture strain of carbon, glass, and basalt FRPs is 8,190, 17,780, and 19,370 με, respectively. These values will be compared to the measured rupture strain of the corresponding

FRP jackets. Moreover, four dog bone shape epoxy specimens were prepared and tested per ASTM D638 [42]. The tensile strength and modulus of the epoxy after a curing time of 7 days at a temperature of 22 °C were measured as 34.6 MPa and 3.39 GPa, respectively. Details of the procedure can be found in Das [43].

2.3. FRP Jacket Preparation

This section describes the FRP wrapping procedure used to prepare FRP jackets for the ICE test. Dry fabrics were cut to the correct dimensions, depending on the number of layers being applied. The length of the dry fabric is the external circumference of FRP wrap multiplied by the number of layers of FRP, plus an overlap length of half of the FRP cylinder circumference. PVC pipes of different diameters were used as molds for wrapping the fabrics fully around the circumference. The pipes were covered with wax paper so that the wrapped FRP can be removed easily from the mold after curing. A wet lay–up procedure was used to prepare the FRP jackets. According to the manufacturer's recommendations, the epoxy and its hardener were combined at a weight ratio of 100:34.5 and were mixed with an electric mixer for 5 minutes. The epoxy was also thickened by mixing with a small quantity of Cabosil TS-720 Fumed Silica to prevent dripping and to ensure that the epoxy remained on the fiber until it cured.

As shown in Figure 1, a small amount of epoxy was poured on the plastic surface and the fabric sheet was placed on top. Using a plastic trowel, the fabric was pressed gently into the epoxy. The trowel was pressed firmly enough for the epoxy to completely penetrate the dry fabrics but not bend or crease them. The movement of the trowel was maintained parallel to the fiber direction. Additional epoxy was added to the top of the fabric sheet as needed, until the fabric was fully saturated. The PVC pipe covered with wax paper was placed horizontally at the edge of the FRP and the length of the fiber sheet was rolled onto the pipe having the unidirectional fibers in the

circumference direction. During the wrapping process, a constant tensile stress was maintained and a trowel was used to remove any air bubbles within the wrap. A plastic strip was attached to the end of the overlap portion to restrict it from peeling away while curing. The specimens were supported by a rod inside the pipe oriented horizontally so that the FRP does not sag due to self-weight prior to curing. The specimens were left to cure for 7 days at room temperature (22 °C). After curing, the PVC pipe was fixed in a vice clamp and the FRP jacket was pulled off the mold. The FRP jackets were cut to the final length with a band saw. An aspect ratio of 2:1 (height to diameter) was adopted to minimize the effect of end boundaries on failure of the FRP jacket.

2.4. Test Setup and Instrumentation

In the ICE test method, as proposed by De Caso y Basalo et al. [38], an internal hydrostatic pressure is applied to a cylindrical FRP jacket using freezing water. The ICE test rig, as schematically illustrated in Figure 2, consists of two square steel plates with concentric grooves machined on one side of each to accommodate the open-ended FRP cylinders of different diameter. The grooves had an appropriate width to accommodate the varying thicknesses of the FRP jackets due to the number of layers for a given cylinder diameter. The steel plates were drilled with aligned circular holes at each corner to accommodate threaded steel rods. The rods were fixed to the plates with washers and bolts. In addition, the top-plate was drilled with a 16-mm diameter hole to insert a valve in order to fill and seal the rig. The fixture formed a frame designed to restrict movement in the longitudinal direction, allowing only radial displacement between the plates. The sizes of the steel rods and plates were calculated according to the maximum expected hydrostatic pressure exerted by frozen water. The pressure was calculated theoretically considering an adiabatic bulk modulus K for water of 700 MPa. Threaded rods of grade 60 ksi (410 MPa) steel were used. Multiple rigs were manufactured for each of the different FRP jacket diameters.

The FRP jacket was placed vertically within the groove of the bottom plate, sealed with waterproof silicon, and allowed to air cure for 12 hours. To check for possible leaks through the silicon seal or the specimen, the jacket was filled with tap-water at room temperature. In the case of leaks, the bottom seals were reapplied, or voids in the FRP jacket were patched with a thin layer of epoxy. The top plate was then fitted to the open end of the jacket and sealed with silicon. The steel plates were aligned using the high-strength steel threaded rods bolted with equal torque to ensure uniform and symmetric compression of the seal. The FRP jackets were typically instrumented with two strain gauges oriented to measure the hoop strain. The strain gauges were located at the mid height of the jacket, one in the middle of the overlapped region and another one 180° apart. Selected specimens were instrumented with five strain gauges to capture the distribution of hoop strain around the circumference of the FRP jacket at mid height. The test setup was then placed in an environmental chamber and a K-type thermocouple was attached to the surface of the FRP to record the temperature of the specimen. The strain gauges and thermocouple were connected to a data acquisition system to record the hoop strain along with the temperature of the FRP cylinder. The temperature of the environmental chamber was maintained at 0 °F (-17.8 °C). The specimens were left in the chamber until failure. The time for FRP rupture varied from 1-8 hours depending on the size of the FRP jackets.

2.5. Test Matrix

A total of 45 jacket specimens were prepared and tested. As shown in Table 3, each specimen is given an identification (ID) label as F-DX-LY-N, where F stands for fiber type (C: carbon, G: glass, and B: basalt), DX stands for inner diameter of jacket (D60: 60.3 mm, D114: 114.3 mm, and D216: 215.9 mm), LY stands for number of FRP layers (L1: 1 layer, L2: 2 layers, and L3: 3 layers), and N stands for specimen number (1, 2, and 3). For example, C-D60-L2-3 is a jacket specimen

made of carbon FRP, inner diameter of 60.3 mm, 2 layers of FRP, and the 3rd replicate of this specimen type. For some combinations, no specimen was prepared (see Table 3). Three specimens of each combination of FRP material and number of layers were tested for the smallest diameter. Observing the consistency of results, only two or one identical specimens were tested for each of the combinations for the remaining diameters.

2.6. Test Results and Discussions

As shown in Table 3, two strain readings at failure condition are provided, namely at location A (in the middle of overlapped region) and location B (in the middle of non-overlapped region). As the overlap length is half of the circumference of each jacket, locations A and B are 180 degrees apart. Figure 3 shows the typical failure of FRP jackets. The failure pattern observed was predominately in the non-overlapped region with a peak measured strain at the thinner side of the FRP jacket (i.e. location B). As shown in Figure 4, linear behavior was observed in the strain-time responses for all specimens up to failure, with some drops in strain due to the release of ice pressure from localized failure of the seals, or longitudinal splitting parallel to the fibers. The maximum strain at failure for location B was relatively less for 2-layered FRP jackets than 1- layered jackets, however 3-layered FRP jackets recorded a higher strain than 2-layered jackets. Overall, the rupture strain values of FRP jackets are consistently lower than the ultimate tensile strain of the corresponding flat coupons shown in Table 2. It should be noted that the focus of the study was the variation of hoop strain, thus no pressure/load cell was implemented in the test and stress data are not available. All strain gauges were installed in the hoop direction. As a result, time is the parameter selected to allow for visualization of hoop strain variation. In general, internal pressure (and thus FRP stress) would increase with test time.

The variation of hoop strain along the circumference of specimen C-D114-L1-1 was recorded using five strain gauges at the mid height of the specimen. Figure 5 shows the hoop strain vs. time response of the FRP jacket with the five strain gauges along with the layout of the strain gauges. As expected, the hoop strain values in the overlapped region of the FRP jacket are lower than strains measured in non-overlapped region. This observation has been already evidenced many times in the literature. The peak strain is observed by strain gauge 3 (i.e. location B of the jackets with two strain gauges), and the lowest values were for strain gauges 1, 4, and 5. Strain gauges 4 and 5 were in the overlapped region and the results were expected. Strain gauge 3 was located at the end of the overlapped region with almost the lowest strain. This might be due to the accumulation of resin at the end of the wrap and installation of the gauge on a thick part of the wrap.

Comparison of the rupture hoop strains of FRP jackets tested by the ICE test method to the rupture stain of corresponding flat coupons indicates a significant premature failure in the FRP jackets. Using Eq. 1, the average stain efficiency factor of each set of jacket specimens was calculated and presented in Table 4. For FRP jackets made of carbon fiber, the strain efficiency factor ranges from 0.53 to 0.98 with an average of 0.69 and standard deviation of 0.17. For FRP jackets made of glass fibers, the strain efficiency factor ranges from 0.61 to 0.79 with an average of 0.71 and standard deviation of 0.09. Finally, for FRP jackets made of basalt fibers, the strain efficiency factor ranges from 0.73 to 1.05 with an average of 0.85 and standard deviation of 0.12. There is no significant difference between carbon, glass, and basalt FRP jackets in term of the average strain efficiency factor, however, variability of the observed results is relatively high. Overall, the strain efficiency factor of all specimens ranges from 0.53 to 1.05 with an average of 0.76 and standard deviation of 0.15. The average strain efficiency factor is slightly higher than

those obtained by other researchers based on FRP-wrapped concrete cylinders. For example, review of a large database [31] of 454 FRP-wrapped concrete cylinders showed that the strain efficiency factor ranges from 0.12 to 1.22 with an average of 0.67, and a very large standard deviation of 0.23. The average observed from the large data set (0.67) is somewhat lower than that observed in the current study (0.76), however, the variability of the current study is also quite a bit less than the large data set (coefficient of variation of 20% for the current study vs. 34% for the large data set).

A key difference between the current study and the large data set is that there is no concrete core in the current study. As such, the circumferential FRP in the current study is likely not subjected to possible stress concentrations that may result with concrete cracking or the bond failure between the core and FRP jacket, and thus, have exhibited a higher average strain efficiency factor as compared to concrete-filled specimens. The axial load condition of FRP jackets tested with the ICE method is also different from jackets loaded with internal concrete cores, which could have some influence on the results. ICE method jackets are close to a neutral state of axial stress, or possibly subjected to slight axial tension as the ice expands, counteracting initial slight axial compression due to the weight of the test setup itself. Specimens tested with concrete cores are subjected to some level of axial compression as the axial load is transferred to both core and jacket and distributed based on the bond and relative stiffness. However, due to the very low transverse stiffness of FRP jackets made of unidirectional fibers, the condition of the jacket in the ICE test method is close to the actual condition of FRP jackets on concrete columns. Overall, the results of the current study indicate that the ICE test method is an effective technique to isolate the effect of the concrete core and the axial load from other parameters such as FRP curvature and bi-axial state

of hoop and radial stresses. The following section provides an in-depth understanding of the latter parameters.

3. ANALYTICAL MODELING

This section covers the development of an analytical model primarily based on the bi-axial state of hoop and radial stress in a cylindrical FRP jacket tested using the ICE test method. The longitudinal stress is ignored as there is no significant longitudinal stress in the jacket. There might be a slight longitudinal compressive stress in the jacket due to tightening the nuts of the steel rods and the self-weight of the top plate, which is negligible compared to the magnitudes of hoop and radial stresses. Further, some of the longitudinal compressive stress is also counteracted by the internal ice pressure pushing against the steel plate and threaded rods. It should be mentioned that the model is developed for FRP jackets made of unidirectional fabrics in the hoop direction and all FRP layers must have the same fiber direction. The effect of fiber orientation [44][45][46] and longitudinal FRPs [47][48] are beyond the scope of this study.

3.1. Description of Model

As shown in Figure 6(a), the radial compressive stress σ_r is applied to the FRP jacket as water changes from liquid to ice and its volume increases. Due to the radial stress, a hoop tensile stress σ_θ is developed in the FRP jacket. It is assumed that the radial stress is uniform and no shear stress is developed between the ice and FRP. It should be noted that the radial stress is maximum at the inner surface of the jacket and gradually decreases to zero at the outer surface. As a result, the maximum bi-axial state of stress occurs at the inner surface and as soon as it reaches the bi-axial failure criteria, the inner surface rupture will instantaneously propagate through the jacket thickness towards the outer surface as all fibers are oriented in the hoop direction. For a jacket

made of unidirectional FRPs in the hoop direction, the hoop and radial strains at the inner layer of the jacket can be given as follows:

$$\varepsilon_\theta = \frac{\sigma_\theta}{E_1} + v_{21}\frac{\sigma_r}{E_2} \qquad (2)$$

$$\varepsilon_r = \frac{\sigma_r}{E_2} + v_{12}\frac{\sigma_\theta}{E_1} \qquad (3)$$

where ε_θ is the hoop strain, ε_r is the radial strain, E_1 is the elastic modulus in the hoop (i.e. fiber) direction, E_2 is the elastic modulus in the radial (i.e. matrix) direction, v_{12} is the major Poisson's ratio, and v_{21} is the minor Poisson's ratio of FRP. It is assumed that positive stress and strain are tensile in the hoop direction and compressive in the radial direction. This assumption eliminates the conventional negative signs in the second terms of Eqs. 2 and 3 and simplifies the rest of formulation, as the hoop stress is always tensile and the radial stress is always compressive in the current problem. For half of the cylindrical jacket, as shown in Figure 6(b), equilibrium of the hoop and radial forces can be used to drive the relationship between the radial and hoop stresses as follows:

$$\sigma_r = \frac{2t}{D}\sigma_\theta \qquad (4)$$

where D is the inner diameter of the cylindrical FRP jacket and t is the thickness of the FRP. It is believed that the presence of the radial compressive stress reduces the strength of the FRP jacket in the hoop direction, and a bi-axial strength failure criterion should be considered for this case. The most widely used criterion for FRP composites is the Tsai-Wu interactive tensor polynomial theory [49], which provides an elliptical failure envelope in the bi-axial stress plane. The details of the failure theory were previously described by Fam and Rizkalla [50] and Sadeghian and Fam [31]. A quadrant of the Tsai-Wu failure envelope for two typical unidirectional FRP composites adopted from Daniel and Ishai [51] are presented in Figure 7. As the elliptical Tsai-Wu failure

envelope needs many mechanical parameters of the FRP jacket typically not available to the design engineer, a simplified linear failure envelope is proposed as follows:

$$\frac{\sigma_r}{\sigma_{ru}} + \frac{\sigma_\theta}{\sigma_{\theta u}} = 1 \tag{5}$$

where $\sigma_{\theta u}$ is the uniaxial tensile strength of FRP in the fiber direction and σ_{ru} is the uniaxial compressive strength of FRP in the matrix direction. The proposed failure envelope is plotted in Figure 7 as dotted straight lines for the two typical unidirectional FRP composites and compared with the original Tsai-Wu envelope. The figure shows that the proposed linear envelope has a relatively good agreement with the Tsai-Wu envelope. Moreover, the proposed linear envelope is located inside the Tsai-Wu's safe region. As such, models based on this linear approximation would lead to a safe design. This provides the basis to rationalize the reduced hoop rupture strain observed in the ICE test method by taking the hoop stress σ_θ and the radial stress σ_r from Eqs 4 and 5, substituting them into Eq. 2, and using $E_1/E_2 = v_{12}/v_{21}$ resulting in the following:

$$\varepsilon_\theta = \frac{\frac{\sigma_{\theta u}}{E_1}\left(\frac{D}{t} + 2v_{12}\right)}{\left(\frac{D}{t} + 2\frac{\sigma_{\theta u}}{\sigma_{ru}}\right)} \tag{6}$$

At the failure condition in the hoop direction of an FRP jacket, the hoop strain ε_θ reaches the effective hoop strain ε_{fe}, while the rupture strain of the flat coupon is $\varepsilon_{fu} = \sigma_{\theta u}/E_1$. Hence, Eq. 6 can be rewritten in the form of the strain efficiency factor κ_ε as follows:

$$\kappa_\varepsilon = \frac{\frac{D}{t} + 2v_{12}}{\frac{D}{t} + 2\beta} \tag{7}$$

where β is the ratio of the axial tensile strength $\sigma_{\theta u}$ (i.e. in the fiber direction) to the transverse compressive strength σ_{ru} (i.e. in the matrix direction) of the unidirectional FRP composite used for the jacket. It should be noted that the proposed analytical model given by Eq. 7 is based on the bi-

axial hoop and radial stresses in FRP jackets tested using the ICE test method. As highlighted previously, in the case of concrete columns wrapped with FRPs, there may be additional factors affecting the strain efficiency of the FRP jacket.

3.2. Comparison to Test Data

Equation 7 was used to predict the hoop rupture strain and strain efficiency factor of 18 different cylindrical FRP jackets tested in this study as presented in Table 4. In addition, a second set of 9 different cylindrical FRP jackets tested by De Caso y Basalo et al. [38] using the ICE test method are added to the table. In the second set of test data, a total of 54 glass FRP jackets with three different internal diameters, namely 60, 115 and 171 mm; and one-, two-, and three-plies were tested. Six jackets for each combination were tested and the average hoop rupture strains were reported. As presented in Table 4, the stain efficiency factor of the second set ranges from 0.49 to 0.88 with an average of 0.72 and standard deviation of 0.14. These results are comparable to the test results presented in this study.

In order to compute the hoop rupture strain and strain efficiency factor of the test specimens, two required parameters including the major Poisson's ratio v_{12} and the axial/transverse strength ratio β of the FRP jackets are adopted from Daniel and Ishai [51] for typical FRP materials. Per Table 5, for all types of fibers, v_{12} and β are recommended to be taken as 0.28 and 10, respectively, unless more accurate values are available to designers. Using the proposed analytical model, the hoop rupture strain and strain efficiency factor of the test specimens were computed and presented in Table 4. As shown in the table, the predicted strain efficiency factor using the proposed analytical model ranges from 0.45 to 0.91 with an average of 0.70 and standard deviation of 0.13. For comparison, it can be seen that the experimental strain efficiency factor of the entire database ranges from 0.49 to 1.05 with an average of 0.75 and standard deviation of 0.14. The

results show that the model is able to predict the experimental strain efficiency factors with an average error of -3.4%. Figure 8 shows the predicted strain efficiency factors compared to the experimental factors. The data shows good agreement and illustrates that the strain efficiency factor is indeed a variable, as expected.

As the main variable is the FRP jacket diameter to thickness ratio (D/t), the performance of the proposed analytical model needs to be evaluated for different ranges of D/t. Based on the results presented in Table 4 and Figure 8, the average error of the proposed analytical model with respect to the experimental data for D/t <50, 50< D/t <100, and D/t >100 can be calculated as -12.6, -3.7, and +21.2%, respectively. It indicates that the proposed analytical model underestimate cases with D/t <50 and overestimate cases with D/t >100. The best prediction is for cases with 50< D/t <100. Overall, the ability of the proposed analytical model to predict the results of the ICE test method is satisfactory.

3.3. Parametric Study

In this section, a parametric study is performed using the proposed analytical model for the strain efficiency factor of FRP jackets tested with the ICE test method to investigate the effects of the key parameters, namely: (a) FRP jacket diameter/thickness ratio D/t; (b) FRP axial/transverse strength ratio β; and (c) FRP major Poisson's ratio v_{12}. For each parameter, the objective is to study the variation of the strain efficiency factor against that specific parameter. In order to have a better understanding of the effect of each parameter on the x-axis, another parameter (D/t or β) is varied to produce a series of curves for comparison. While two parameters are being investigated, the other parameter is kept constant. The default values are $v_{12} = 0.28$ and $\beta = 10$ in this parametric study.

3.3.1. Effect of FRP Jacket Diameter/Thickness Ratio

The range of FRP jacket diameter/thickness ratio D/t considered in this parametric study was from 10 to 440. It should be noted that the range of D/t ratio available in the experimental database (Table 4) covered values from about 15 to 200. Figure 9(a) shows the variation of strain efficiency factor against D/t for FRP axial/transverse strength ratio β ranging from 5 to 100. As shown, increasing the D/t ratio increases the strain efficiency factor with a non-linear rate; however, the rate of increase is smaller for larger D/t ratios. The strain efficiency factor is also smaller for larger β ratios. For example, at $\beta = 10$, increasing D/t from 20 to 200 resulted in a 78% increase in the strain efficiency factor (i.e., from 0.51 to 0.91); and at $\beta = 20$, it resulted in a 147% increase (i.e., from 0.34 to 0.84). The figure shows that all curves approach the strain efficiency factor of 1.0 as D/t ratio approaches infinity, which corresponds to the flat coupon condition.

Figure 9(a) also shows that the variation of the strain efficiency factor is larger for smaller D/t ratios, which represent small-scale test specimens. For large-scale test specimens and full-scale concrete columns, it is expected to have larger strain efficiency factors. For example, for a 400 mm diameter circular concrete column wrapped with five plies of a unidirectional carbon FRP in the hoop direction (assuming 1 mm thickness of each layer), the D/t ratio is 80. Thus for a typical $\beta = 10$ and $v_{12} = 0.28$, the strain efficiency factor is calculated to be 0.81, which is larger than that of typical small-scale test specimens presented in Table 4. This clearly implies that strain efficiency factors derived from small-scale test specimens are likely to be highly conservative for full-scale applications with large diameter to thickness ratios. Therefore, design recommendations for strain efficiency factor need to consider D/t ratio as an important parameter. This is consistent with the observations of the current study and De Caso y Basalo et al. [38] using the ICE test method, as well as the observations by Luca et al. [52] and Sadeghian and Fam [53] regarding the

scalability of test results from small-scale FRP-wrapped concrete specimens to full-scale design applications. It should be noted that the actual thickness of the FRP jacket should be used in the proposed model. This is important as some researchers report only the nominal FRP thickness.

3.3.2. Effect of FRP Axial/Transverse Strength Ratio

The range of FRP jacket axial/transverse strength ratio β considered in this parametric study was 1 to 50. For example, $\beta = 5$ refers to a unidirectional FRP with the tensile strength in the axial (fiber) direction five times that of the compressive strength in the transverse (matrix) direction. Figure 9(b) shows the variation of strain efficiency factor against β for various D/t ratios ranging from 10 to 400. As shown, increasing β decreases the strain efficiency factor with a non-linear rate; however, the rate of the decrease is larger for smaller β ratios. The strain efficiency factor is smaller for smaller D/t ratios. For example, at $D/t = 20$, increasing β from 5 to 45 resulted in a 72% decrease in the strain efficiency factor (i.e., from 0.68 to 0.19); and at $D/t = 100$, it resulted in a 42% decrease (i.e., from 0.91 to 0.53).

3.3.3. Effect of FRP Major Poisson's Ratio

The range of FRP major Poisson's ratio v_{12} considered in this parametric study was 0 to 0.5. Figure 9(c) shows the variation of strain efficiency factor against v_{12} for various D/t ratios ranging from 10 to 400. As shown, increasing v_{12} increases slightly the strain efficiency factor with a linear rate. For example, at $D/t = 20$, increasing v_{12} from 0.1 to 0.4 resulted in only a 3% increase in strain efficiency factor (i.e., from 0.505 to 0.520); and at $D/t = 100$, it resulted in only a 1% increase (i.e., from 0.835 to 0.840). Overall, the effect of the major Poisson's ratio is insignificant.

3.4. Simplified Model

Some mechanical properties of FRP composites used in civil engineering, such as the compressive strength in the matrix direction and Poisson's ratios, are not typically reported and therefore are

often unknown by the designer. Eliminating those properties from design equations can be helpful, if justified. As concluded in the parametric study, the effect of the major Poisson's ratio on the strain efficiency factor is insignificant. Thus, if v_{12} is removed from the numerator in Eq. 7 as it is very small compared to realistic values of D/t, and if β is taken as 10 to be representative of typical unidirectional FRPs used in civil engineering applications, Eq. 7 may be simplified to the following:

$$\kappa_\varepsilon = \frac{1}{1 + 20\frac{t}{D}} \tag{8}$$

As presented, the simplified proposed model (Eq. 8) for the strain efficiency of FRP jackets tested using the ICE test method is a function of t/D only. The performance of the simplified model is compared to the proposed analytical model in Figure 10. As shown, the simplified model is as good as the analytical model having good agreement with the experimental test results. The results showed that the simplified model predicts the experimental strain efficiency factors in Table 4 with an average error of -4.6%, which is slightly on the conservative side compared to the average error of -3.4% using the analytical model. Interestingly, the strain efficiency factor is related to the curvature of the FRP jacket 1/R, where R is the inner radius of the jacket. In other words, the proposed models in this study account for the effect of the bi-axial hoop and radial stresses directly, as well as the effect of FRP curvature indirectly.

In a different study, Chen et al. [19] investigated the effect of FRP curvature in a split-disk test. It was concluded that local strains are increased by circumferential bending of the FRP ring at the gap of the split-disk due to change of curvature there caused by the relative movement of the two half disks. The FRP ruptures once the strain at one of these locations reaches the FRP coupon rupture strain, leading to a lower apparent tensile strength than that obtained from flat

coupon tests. In order to predict the results of the split-disk test, Chen et al. [19] recommended a strain reduction factor given by the following:

$$\rho = \frac{\varepsilon_{rup}}{\varepsilon_{rup} + \dfrac{t}{2R}} \tag{9}$$

where ε_{rup} is the rupture strain obtained from the flat coupon test. As presented, in terms of the effect of t/D, there is a similarity between the proposed simplified model (i.e. Eq. 8) in this study and the model (i.e. Eq. 9) recommended by Chen et al. [19]. However, the models were derived in two completely different domains.

It should be highlighted that the proposed model is based on FRP jackets tested by the ICE test method. As explained earlier, the authors believe that the bi-axial effect is one of the factors affecting the premature rupture of hoop fibers for FRP-wrapped concrete columns. The proposed model quantifies only the bi-axial state of radial and hoop stresses in a FRP jacket. It is believed that the concrete core also affects the value of the strain efficiency factors. As the proposed model does not account for the presence of concrete, it should not be directly used for design applications. For the case of FRP-wrapped concrete columns, the effects of longitudinal stress, stress localization due to cracking of the concrete core, fiber misalignment, and over-lap region should also be accounted for. Some of the parameters might interact with others, thus their possible synergy should also be considered. The current study showed that the effect of the bi-axial state of radial and hoop stresses is a major factor. Moreover, the current study showed that the curvature of the FRP jacket (D/t) and the bi-axial state of radial and hoop stresses are related to each other. In other words, the effect of FRP curvature was indirectly considered in the current study. Further studies may focus on quantifying the effect of other parameters and possible interaction between them for design applications.

4. CONCLUSION

A total of 45 cylindrical FRP jackets were manufactured using three unidirectional fabrics (carbon, glass and basalt) with three different internal diameters (60, 114, and 216 mm) and three different numbers of layers (1, 2, and 3). The FRP jackets were tested using the ICE method. The average hoop rupture strain of FRP jackets were obtained and compared to the rupture strain of corresponding flat coupons. The ratio of the rupture strain was implemented in the form of a strain efficiency factor. A new analytical model was developed to quantify the strain efficiency factor of the FRP jackets. The model implemented the bi-axial state of stress in the FRP jacket under a tensile stress in the hoop direction and a compressive stress in the radial direction. The analytical model engaged four major parameters, namely: diameter, FRP thickness, axial/transverse strength ratio, and major Poisson's ratio of the FRP jacket. The two latter parameters were eliminated after a parametric study to propose a simplified formula as a function of the diameter/thickness ratio only. The models were verified against the experimental results. The following conclusions can be drawn from the study:

- Comparison of the rupture hoop strains of FRP jackets tested using the ICE test method to the rupture stain of corresponding flat coupons indicated a significant premature failure in the FRP jackets. The failure pattern observed was predominately in the non-overlapped region of the FRP jacket.

- No significant difference between carbon, glass, and basalt FRP jackets were observed in terms of failure and strain efficiency. Overall, the strain efficiency factor of the test specimens in this study ranged from 0.53 to 1.05 with an average of 0.76 and standard deviation of 0.15.

- Adding another set of test data from an independent study resulted in an experimental strain efficiency factor ranging from 0.49 to 1.05 with an average of 0.75 and standard deviation of 0.14.

- The experimental results indicated that the ICE test method is an effective technique to examine the hoop strain and failure mode of cylindrical FRP jackets.

- The proposed analytical model predicted the strain efficiency factor of the specimens ranging from 0.45 to 0.91 with an average of 0.70 and standard deviation of 0.13; which are comparable to the experimental values. The results clearly showed that the strain efficiency factor was indeed a variable. The results also showed that the analytical model was able to predict the experimental strain efficiency factors with an average error of -3.4%.

- A parametric study on the diameter/thickness ratio, the axial/transverse strength ratio, and Poisson's ratio of the FRP jacket showed that the diameter/thickness ratio was a major factor regarding the strain efficiency factor.

- The parametric study resulted in a simplified formula as a function of the diameter/thickness ratio (i.e. curvature of FRP jacket) only. The simplified model was also verified against the experimental results with an average error of -4.6%.

- The study was intended to provide a rational explanation for the reduced hoop rupture strains of FRP jackets tested using the ICE test method. More studies are needed for FRP-wrapped concrete columns to consider the effect of other contributing factors including the effects of longitudinal stress, stress localization, fiber misalignment, and over-lap region as well as their possible synergies.

5. ACKNOWLEDGEMENTS

6. REFERENCES

[1]   Saadatmanesh, H., Ehsani, M. R., and Li, M. W. (1994). Strength and ductility of concrete columns externally reinforced with fiber composite straps. ACI Structural journal, 91(4), 434-447.

[2]   Mirmiran, A., and Shahawy, M. (1997). Behavior of concrete columns confined by fiber composites. Journal of Structural Engineering, 23(5), 583–590.

[3]   Teng JG, Chen JF, Smith ST, and Lam L. (2003). Behaviour and strength of FRP-strengthened RC structures: a state-of-the-art review. Proceedings of the institution of civil engineers-structures and buildings, 156(1), 51-62.

[4]   Bakis C, Bank LC, Brown V, Cosenza E, Davalos JF, Lesko JJ, Machida A, Rizkalla SH, and Triantafillou TC. (2002). Fiber-reinforced polymer composites for construction-state-of-the-art review. Journal of Composites for Construction, 6(2), 73-87.

[5]   Motavalli M, and Czaderski C. (2007). FRP composites for retrofitting of existing civil structures in Europe: state-of-the-art review. International Conference of Composites & Polycon., American Composites Manufacturers Association. Tampa, FL, USA.

[6]   Hollaway LC. (2012). A review of the present and future utilisation of FRP composites in the civil infrastructure with reference to their important in-service properties. Construction and Building Materials, 24(12), 2419-45.

[7]   Spoelstra, M. R., and Monti, G. (1999). FRP-confined concrete model. Journal of composites for construction, 3(3), 14-150.

[8]   Toutanji, H. (1999). Stress-strain characteristics of concrete columns externally confined with advanced fiber composite sheets. ACI Materials Journal, 96(3), 397-404.

[9]   Shahawy, M., Mirmiran, A., and Beitelman, T. (2000). Tests and modeling of carbon-wrapped concrete columns. Composites Part B: Engineering, 31(6), 471-480.

[10]   De Lorenzis, L., and Tepfers, R. (2003). Comparative study of models on confinement of concrete cylinders with fiber-reinforced polymer composites. Journal of Composites for Construction, 7(3), 219–237.

[11]   Youssef, M. N., Feng, M. Q., and Mosallam, A. S. (2007). Stress–strain model for concrete confined by FRP composites. Composites Part B: Engineering, 38(5), 614-628.

[12]   Matthys, S., Toutanji, H., Audenaert, K., and Taerwe, L. (2005). Axial load behavior of large-scale columns confined with fiber-reinforced polymer composites. ACI Structural Journal, 102(2), 258-267.

[13]   Lam, L., and Teng, J. G. (2003). Design-oriented stress–strain model for FRP-confined concrete. Construction and building materials, 17(6), 471-489.

[14]   Pessiki, S., Harries, K. A., Kestner, J. T., Sause, R., and Ricles, J. M. (2001). Axial behavior of reinforced concrete columns confined with FRP jackets. Journal of Composites for Construction, 5(4), 237-245.

[15]   Nanni, A., and Bradford, N. M. (1995). FRP jacketed concrete under uniaxial compression. Construction and Building Materials, 9(2), 115-124.

[16]   Matthys, S., Taerwe, L., and Audenaert, K. (1999). Tests on axially loaded concrete columns confined by fiber reinforced polymer sheet wrapping. ACI Special Publication, 188.

[17]   Harries, K. A., and Kharel, G. (2003). Experimental investigation of the behavior of variably confined concrete. Cement and Concrete research, 33(6), 873-880.

[18]   Mandal, S., Hoskin, A., and Fam, A. (2005). Influence of concrete strength on confinement effectiveness of fiber-reinforced polymer circular jackets. ACI Structural Journal, 102(3), 383-392.

[19]   Chen, J. F., Li, S. Q., Bisby, L. A., and Ai, J. (2011). FRP rupture strains in the split-disk test. Composites Part B, 42(4), 962–972.

[20]   Harries, K. A., and Carey, S. A. (2003). Shape and "gap" effects on the behavior of variably confined concrete. Cement and Concrete Research, 33(6), 881-890.

[21]   Smith, S. T., Kim, S. J., and Zhang, H. (2010). Behavior and effectiveness of FRP wrap in the confinement of large concrete cylinders. Journal of Composites for Construction, 14(5), 573–582.

[22]   Bisby, L. A., Dent, A. J., and Green, M. F. (2005). Comparison of confinement models for fiber-reinforced polymer-wrapped concrete. ACI Structural Journal, 102(1), 62-72.

[23]   De Lorenzis, L., and Tepfers, R. (2003). Comparative study of models on confinement of concrete cylinders with fiber-reinforced polymer composites. Journal of Composites for Construction. 7(3), 219-237.

[24]   Xiao, Y., and Wu, H. (2000). Compressive behavior of concrete confined by carbon fiber composite jackets. Journal of Materials in Civil Engineering, 12(2), 139-146.

[25] Carey, S. A., and Harries, K. A. (2005). Axial behavior and modeling of small-, medium-, and large-scale circular sections confined with CFRP jackets. ACI Structural Journal, 102(4), 596–604.

[26] Carey, S. (2003). Effects of Shape, 'Gap,' and Scale on the Behavior and Modeling of Variably Confined Concrete. MSc thesis, University of South Carolina, Columbia, SC, USA.

[27] American Concrete Institute. (2017). Guide for the design and construction of externally bonded FRP systems for strengthening concrete structures. ACI 440.2R-17, Farmington, MI, USA.

[28] Bisby, L. A., and Take, W. A. (2009). Strain localisations in FRP-confined concrete: new insights. Proceedings of the ICE-Structures and Buildings, 162(5), 301-309.

[29] Wu, Y. F., and Jiang, J. F. (2013). Effective strain of FRP for confined circular concrete columns. Composite Structures, 95, 479-491.

[30] El-Hacha, R., and Abdelrahman, K. (2013). Slenderness effect of circular concrete specimens confined with SFRP sheets. Composites Part B: Engineering, 44(1), 152-166.

[31] Sadeghian, P., and Fam, A. (2014). A rational approach toward strain efficiency factor of fiber-reinforced polymer-wrapped concrete columns. ACI Structural Journal, 111(1), 135-144.

[32] Lam, L., and Teng, J. G. (2004). Ultimate condition of fiber reinforced polymer-confined concrete. Journal of Composites for Construction, 8(6), 539-548.

[33] Chen, J. F., Li, S. Q., and Bisby, L. A. (2012). Factors affecting the ultimate condition of FRP-wrapped concrete columns. Journal of Composites for Construction, 17(1), 67-78.

[34] Vincent, T., and Ozbakkaloglu, T. (2015). Influence of overlap configuration on compressive behavior of CFRP-confined normal-and high-strength concrete. Materials and Structures, 1-24.

[35] Pham, T. M., Hadi, M. N., and Youssef, J. (2015). Optimized FRP Wrapping Schemes for Circular Concrete Columns under Axial Compression. Journal of Composites for Construction, 04015015.

[36] Fraldi, M., Nunziante, L., Carannante, F., Prota, A., Manfredi, G., and Cosenza, E. (2008). On the prediction of the collapse load of circular concrete columns confined by FRP. Engineering Structures, 30(11), 3247-3264.

[37] Lignola, G. P., Nardone, F., Prota, A., and Manfredi, G. (2012). Analytical model for the effective strain in FRP-wrapped circular RC columns. Composites Part B: Engineering, 43(8), 3208-3218.

[38] De Caso y Basalo, F. J., Matta, F., and Nanni, A. (2011). "Novel test method for ultimate hoop-strain characterization in FRP jackets." Journal of Materials in Civil Engineering, 23(12), 1633-1641.

[39] Fyfe Company. (2016). "Tyfo® SCH-41 Composite using Tyfo® S Epoxy." ⟨http://www.fyfeco.com/Products/~/media/Files/Fyfe/2013-Products/Tyfo%20SCH-41.ashx⟩ (Apr. 19, 2016).

[40] Fyfe Company. (2016). "Tyfo® SEH-51A Composite using Tyfo® S Epoxy." ⟨http://www.fyfeco.com/~/media/Files/Fyfe/2013-Products/Tyfo%20SEH-51A%20Composite.ashx?la=en⟩ (Apr. 19, 2016).

[41]   ASTM D3039 (2008). Standard Test Method for Tensile Properties of Polymer Matrix Composite Materials, American Society for Testing and Materials, West Conshohocken, PA, USA.

[42]   ASTM D638 (2010). Standard test method for tensile properties of plastics. American Society for Testing and Materials, American Society for Testing and Materials, West Conshohocken, PA, USA.

[43]   Das, B. (2014). Variation of hoop strain in fiber reinforced polymer wraps. Master's thesis, North Carolina State University, Raleigh, North Carolina, USA.

[44]   Parvin, A., and Jamwal, A. S. (2005). Effects of wrap thickness and ply configuration on composite-confined concrete cylinders. Composite structures, 67(4), 437-442.

[45]   Sadeghian, P., Rahai, A. R., and Ehsani, M. R. (2010). Effect of fiber orientation on compressive behavior of CFRP-confined concrete columns. Journal of Reinforced Plastics and Composites, 29(9), 1335-1346.

[46]   Vincent, T., and Ozbakkaloglu, T. (2013). Influence of fiber orientation and specimen end condition on axial compressive behavior of FRP-confined concrete. Construction and Building materials, 47, 814-826.

[47]   Mostofinejad, D., and Torabian, A. (2016). Experimental study of circular RC columns strengthened with longitudinal CFRP composites under eccentric loading: comparative evaluation of EBR and EBROG methods. Journal of Composites for Construction, 20(2), 04015055.

[48]   Sadeghian, P. and Fam, A. (2015). Strengthening slender reinforced concrete columns using high-modulus bonded longitudinal reinforcement for buckling control. Journal of Structural Engineering, 141(4), 04014127.

[49]   Tsai, S. W., and Wu, E. M. (1971). A general theory of strength for anisotropic materials. Journal of Composite Materials, 5(1), 58–80.

[50]   Fam, A. Z., and Rizkalla, S. H. (2001). Confinement model for axially loaded concrete confined by FRP tubes. ACI Structural Journal, 98(4), 251–461.

[51]   Daniel, I. M., and Ishai, O. (2006). Engineering mechanics of composite materials. Oxford University Press, New York, NY.

[52]   Luca, A. D., Nardone, F., Matta, F., Nanni, A., Lignola, G. P., and Prota A. (2011). Structural evaluation of full-scale FRP-confined reinforced concrete columns. Journal of Composites for Construction, 15(1), 112-123.

[53]   Sadeghian, P., and Fam, A. (2015). Improved design-oriented confinement models for FRP-wrapped concrete cylinders based on statistical analyses. Engineering Structures, 87, 162-182.

Table 1. Strain efficiency factor of FRP-wrapped concrete columns/cylinders reported in the literature

Reference	Test/database description	Strain efficiency factor
Lam and Teng [13]	Small-scale concrete cylinders wrapped with carbon, aramid, and glass FRPs	0.59 to 0.63
Carey and Harries [25]	Medium- and large-scale columns	0.57 to 0.61
Bisby and Take [28]	Small-scale concrete cylinders wrapped with carbon FRPs	0.73 to 1.04
Carey [26]	251 small-scale concrete cylinders wrapped with FRPs	0.26 to 1.06
Sadeghian and Fam [31]	454 concrete cylinders wrapped with unidirectional FRPs	0.12 to 1.22

Table 2. Flat coupon tensile test results

Fiber type	FRP layers	Tensile strength (MPa)		Elastic Modulus (GPa)		Rupture strain (με)	
		Mean	SD	Mean	SD	Mean	SD
Carbon	1	717	111	89.1	2.9	8030	1000
	2	810	20	97.2	5.3	8350	480
	All	**764**	**88**	**93.2**	**5.9**	**8190**	**720**
Glass	1	439	14	20.5	1.1	21430	1410
	2	292	41	20.7	0.9	14120	1940
	All	**365**	**85**	**20.6**	**0.9**	**17780**	**4280**
Basalt	1	196	11	9.2	0.6	21480	2010
	2	184	16	10.8	1.0	17250	2940
	All	**190**	**14**	**10.0**	**1.1**	**19370**	**3240**

Table 3. Test matrix and results

D (mm)	Carbon FRP jacket			Glass FRP jacket			Basalt FRP jacket		
	Specimen ID	Strain at A (με)	Strain at B (με)	Specimen ID	Strain at A (με)	Strain at B (με)	Specimen ID	Strain at A (με)	Strain at B (με)
1 layer of FRP									
60	C-D60-L1-1	3750	5790	G-D60-L1-1	6750	11300	B-D60-L1-1	7580	18540
	C-D60-L1-2	7100	10480	G-D60-L1-2	12820	13300	B-D60-L1-2	8670	17330
	C-D60-L1-3	2980	7690	G-D60-L1-3	12710	17310	B-D60-L1-3	7870	15790
114	C-D114-L1-1	3490	4090	G-D114-L1-1	12170	15530	B-D114-L1-1	14230	15530
	C-D114-L1-2	1710	5100	G-D114-L1-2	7360	12590	B-D114-L1-2	8180	15020
216	C-D216-L1-1	NA	7990	G-D216-L1-1	NA	NA	B-D216-L1-1	11760	14350
2 layers of FRP									
60	C-D60-L2-1	4770	4500	G-D60-L2-1	4610	10000	B-D60-L2-1	12710	16950
	C-D60-L2-2	1010	4200	G-D60-L2-2	5790	10910	B-D60-L2-2	8480	18360
	C-D60-L2-3	610	4400	G-D60-L2-3	6730	12880	B-D60-L2-3	3990	10670
3 layers of FRP									
60	C-D60-L3-1	3190	3870	G-D60-L3-1	11620	12500	B-D60-L3-1	6610	20290
	C-D60-L3-2	NA	NA	G-D60-L3-2	7180	10150	B-D60-L3-2	NA	NA
	C-D60-L3-3	4340	5500	G-D60-L3-3	8020	9610	B-D60-L3-3	12570	18660
114	C-D114-L3-1	5420	7110	G-D114-L3-1	11090	12730	B-D114-L3-1	12240	15400
	C-D114-L3-2	2170	5550	G-D114-L3-2	11230	12830	B-D114-L3-2	10570	15630
216	C-D216-L3-1	NA	6330	G-D216-L3-1	NA	NA	B-D216-L3-1	16190	18770

NA: Not available

Table 4. Comparison of analytical results to experimental data

Fiber type (Ref.)	D (mm)	t (mm)	D/t	Experiment		Model		Error (%)
				Strain ($\mu\varepsilon$)	κ_ε	Strain ($\mu\varepsilon$)	κ_ε	
Carbon (Current Study)	60	1.0	60	7990	0.98	6210	0.76	-22.29
	114	1.0	114	4590	0.56	7000	0.86	52.41
	60	2.0	30	4370	0.53	5010	0.61	14.82
	60	3.0	20	4690	0.57	4220	0.52	-9.99
	114	3.0	38	6330	0.77	5450	0.67	-13.93
	216	3.0	72	6070	0.74	6370	0.78	4.80
Glass (Current Study)	60	1.3	46	13970	0.79	12570	0.71	-10.03
	114	1.3	88	14060	0.79	14570	0.82	3.66
	60	2.6	23	11260	0.63	9780	0.55	-13.20
	60	3.9	15	10760	0.61	8030	0.45	-25.31
	114	3.9	29	12730	0.72	10770	0.61	-15.40
Basalt (Current Study)	60	1.0	60	17220	0.89	14680	0.76	-14.76
	114	1.0	114	14060	0.73	16560	0.86	17.80
	216	1.0	216	14350	0.74	17670	0.91	23.14
	60	2.0	30	15330	0.79	11860	0.61	-22.62
	60	3.0	20	20290	1.05	9980	0.52	-50.82
	114	3.0	38	15520	0.80	12890	0.67	-16.96
	216	3.0	72	18770	0.97	15050	0.78	-19.78
	60	1.0	60	10530	0.56	14250	0.76	35.35
Glass (De Caso y Basalo et al. [38])	115	1.0	115	14920	0.79	16120	0.86	8.03
	171	1.0	171	16130	0.86	16910	0.90	4.87
	60	2.0	30	10990	0.58	11510	0.61	4.73
	115	2.0	58	16130	0.86	14100	0.75	-12.55
	171	2.0	86	16500	0.88	15360	0.82	-6.93
	60	3.0	20	9150	0.49	9680	0.51	5.76
	115	3.0	38	14170	0.75	12550	0.67	-11.39
	171	3.0	57	14140	0.75	14070	0.75	-0.45
	60	1.0	60	7990	0.98	6210	0.76	-22.29
Mean			**63**		**0.75**		**0.70**	**-3.37**

Table 5. Mechanical properties of typical unidirectional FRPs adopted from Daniel and Ishai [51]

Parameter	E-Glass/ Epoxy	S-Glass/ Epoxy	Aramid/ Epoxy	Carbon/ Epoxy (AS4/3501-6)	Carbon/ Epoxy (IM6G/3501-6)
Axial tensile strength (MPa)	1140	1725	1400	2280	2240
Transverse compressive strength (MPa)	128	158	158	228	215
Fiber volume ratio	0.55	0.5	0.6	0.63	0.66
Major Poisson's ratio, v_{12}	0.28	0.29	0.34	0.27	0.31
Axial/transverse strength ratio, β	8.9	10.9	8.9	10.0	10.4
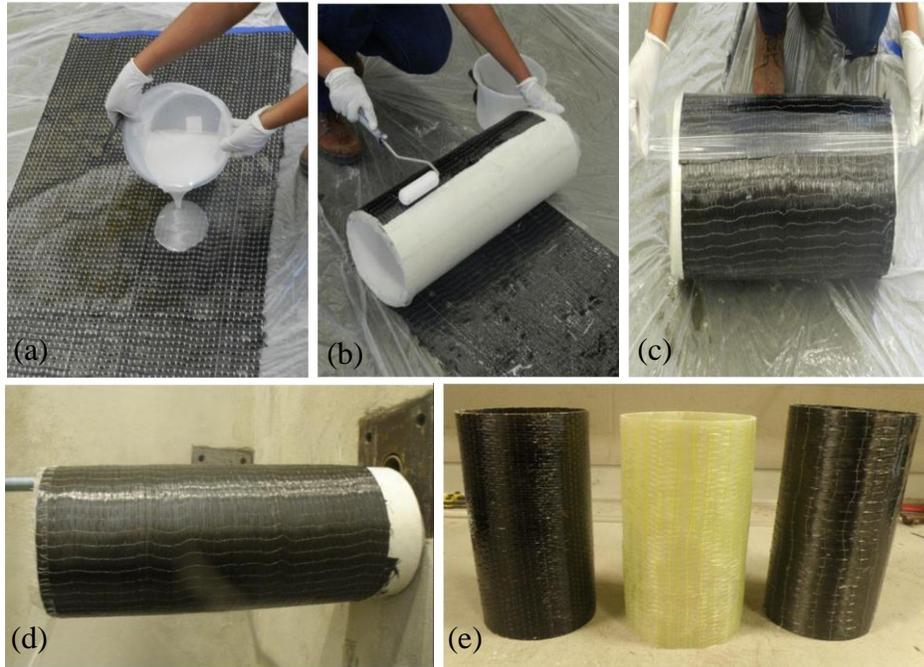
Figure 1. Typical FRP jacket preparation: (a) pouring epoxy on dry fabric, (b) wrapping of saturated fabric on PVC pipe, (c) securing end of fabric by plastic sheet, (d) FRP wrapped pipes curing, and (e) FRP jackets of basalt, glass and carbon (from the left)
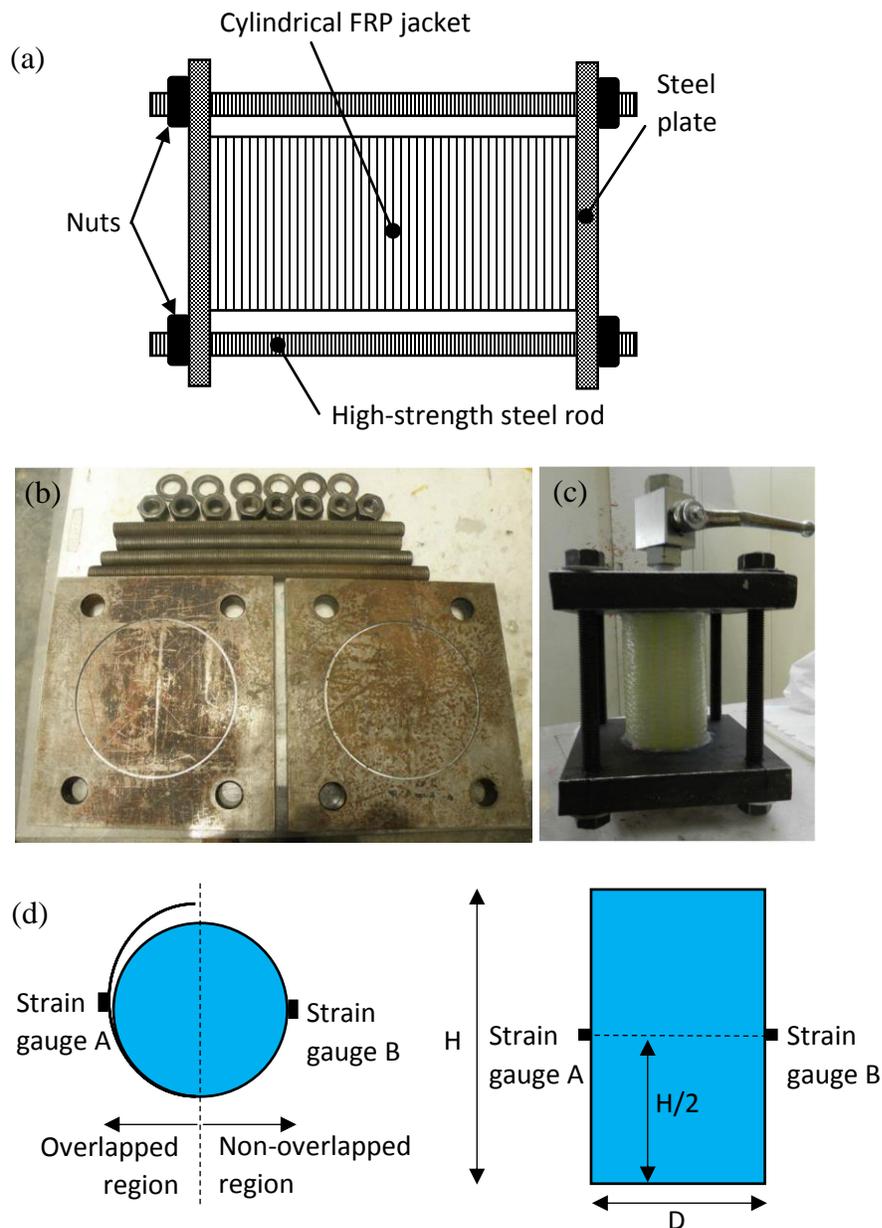
Figure 2. Test setup: (a) schematic setup, (b) rig components, (c) experimental set up, and (d) typical instrumentation

Figure 3. Typical ruptured FRP jackets
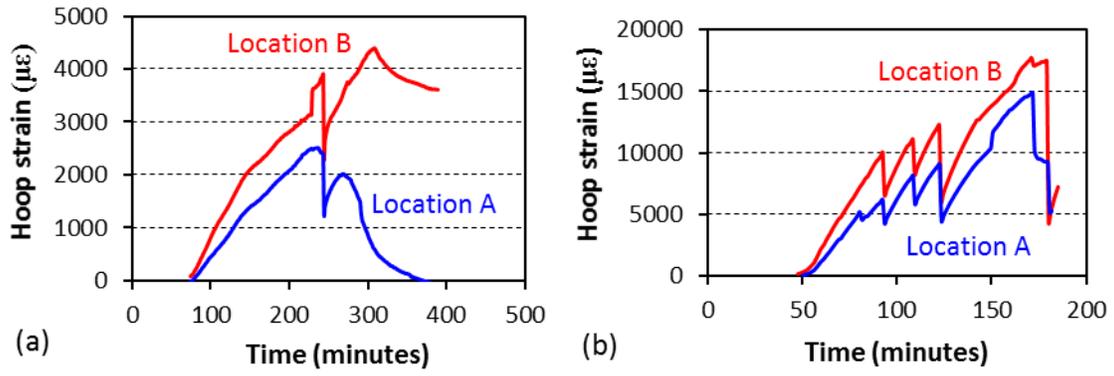
Figure 4. Typical hoop strain vs. time response: (a) C-D60-L2-1 and (b) G-D60-L1-3
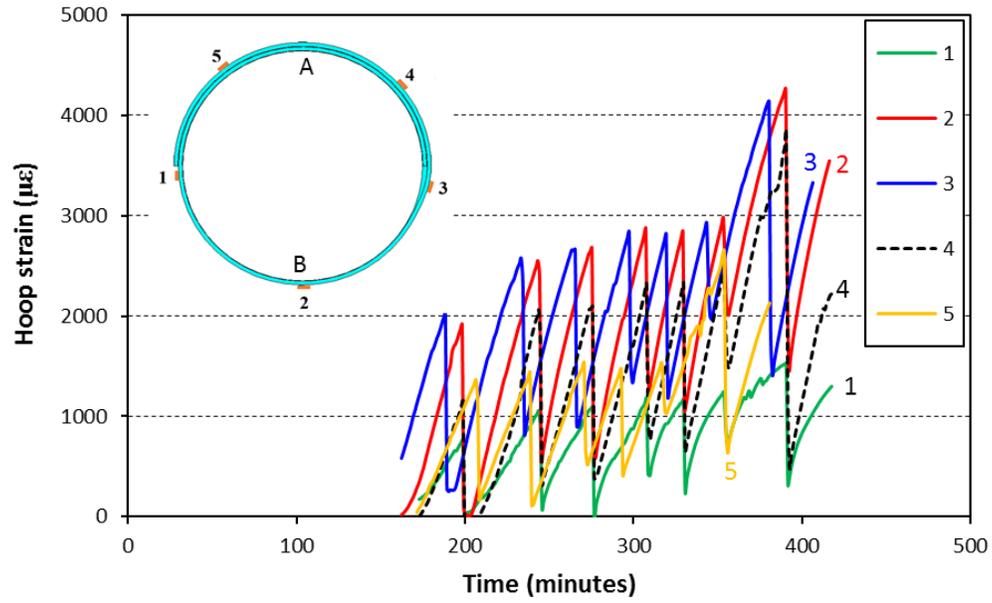
Figure 5. Variation of hoop strain vs. time of specimen C-D114-L1-1 with five strain gauges
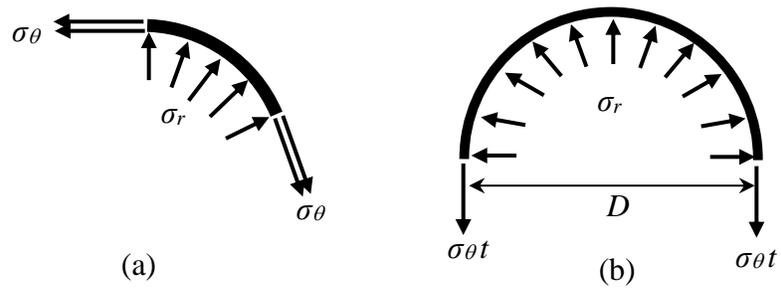
Figure 6. The state of bi-axial radial and hoop stresses in (a) a segment and (b) half of a FRP jacket tested by the ICE test method
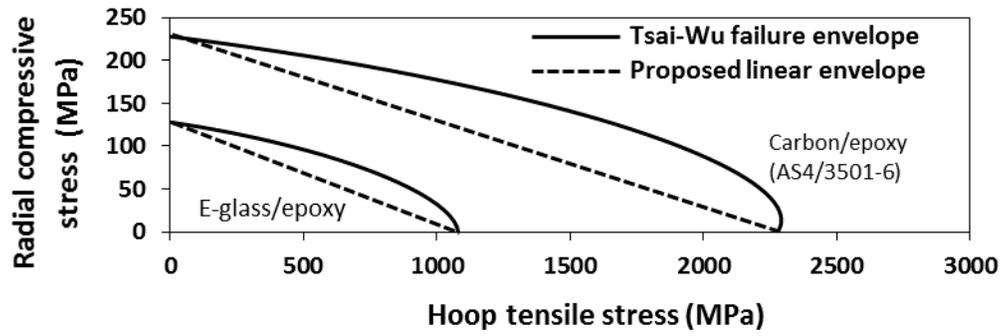
Figure 7. Comparison of simplified linear failure envelope with Tsai-Wu failure envelope for typical unidirectional FRP materials adopted from Daniel and Ishai [51]
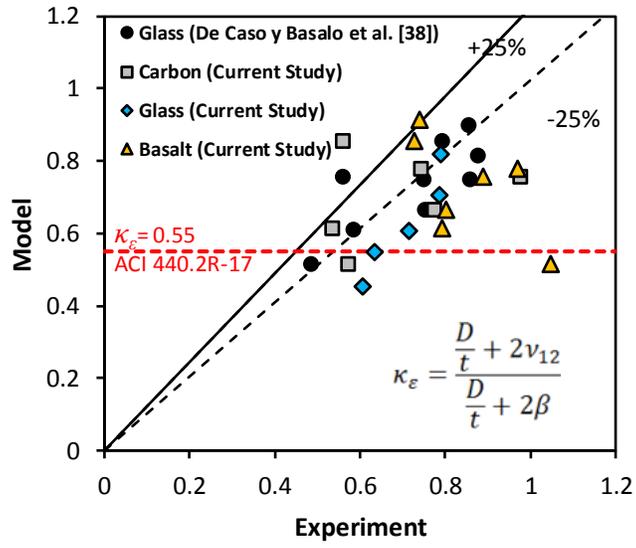
Figure 8. Performance of proposed analytical model against experimental values
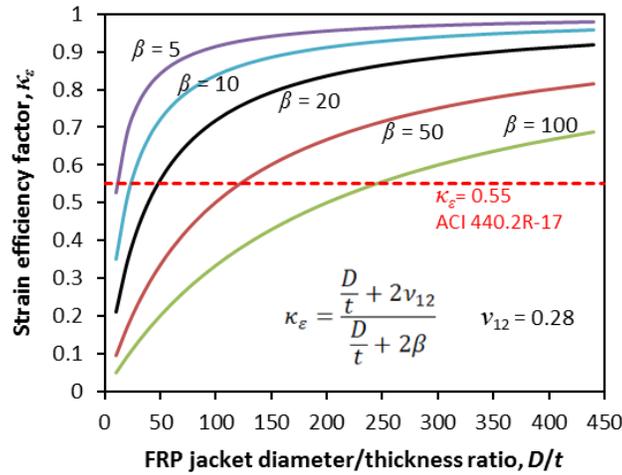
(a)
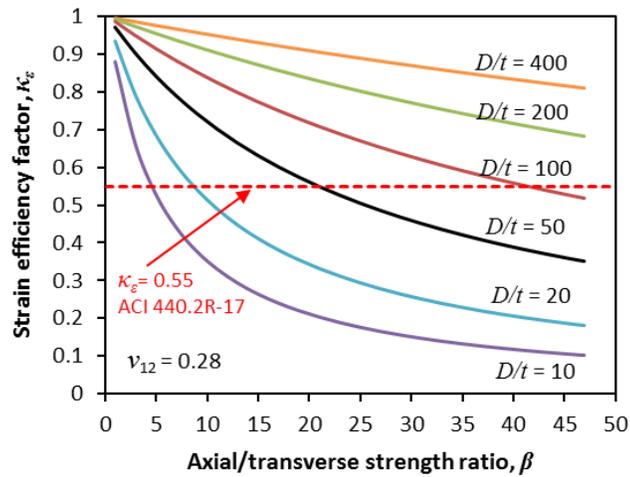
(b)
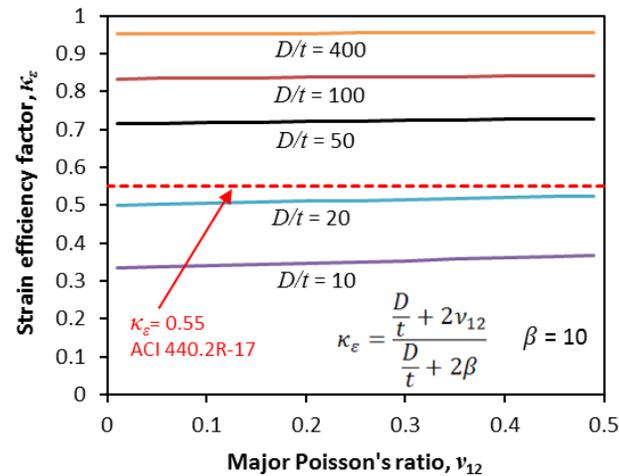
(c)

Figure 9. Effect of (a) FRP jacket diameter/thickness ratio, (b) axial/transverse strength ratio, and (c) major Poisson's ratio on the proposed analytical model for strain efficiency factor
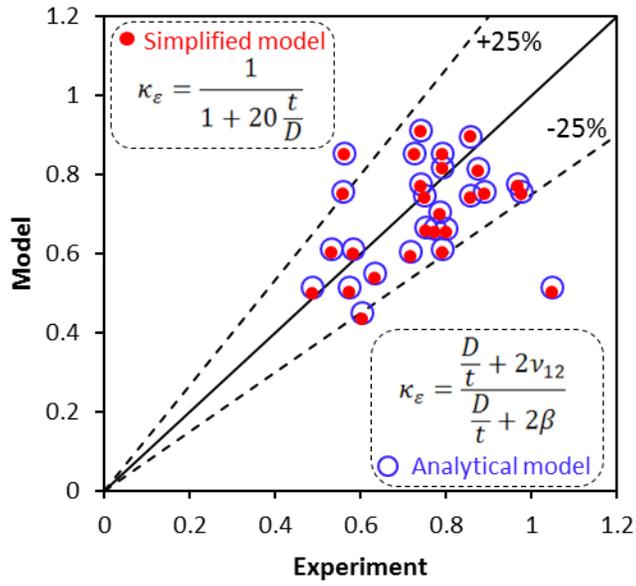
Figure 10. Performance of the simplified model compared to the proposed analytical model and experimental data